Aeroelasticity Research Paper

Composite Wing Design to Account for Flutter

Student: Gavin Fleck	Submitted to: Professor Yuan
Email: gmfleck@wpi.edu	Class: AE6433 Aeroelasticity
Date: 12/1/2025	Assignment: Final Research Paper

1. Introduction

Aircraft wings have developed rapidly over the last 50 years with the integration of composite materials. Historically, for sub-sonic aircraft, wings were made of metals, particularly aluminum for its accessibility, manufacturing, and strength to weight ratio. In working with metals, an isotropic material, engineers often approached design from a structural perspective and then checked aerodynamics. Flutter in aircraft wings is described “as a self-excited oscillation where aerodynamic forces feed energy into the elastic modes of the structure” [1] As aircraft began to move faster, flutter became a greater problem. To overcome this with traditional isotropic materials, engineers sought to make the wings more rigid thereby increasing the natural frequency of the structure and reducing the aeroelastic effects of flutter on the wing.

This approach is still from the structural side of engineering. Composites on the other hand, have opened a door for new possibilities in aeronautical engineering, aeroelastic-tailoring, where engineers can design first for aeroelastic effects such as flutter and use the anisotropy of composite materials to increase flutter speed, while reducing the weight required to do so, and then structurally support the system. “Symmetric lay-up associated with low coupling rigidity is normally undesirable for aeroelastic stability although it has often been employed in real life mainly due to the strength requirement and ease of manufacture.” [2] While standard symmetric lay-ups are common, they often miss the benefits of "bend-twist coupling" which is unique to composites

2. Mechanics of Composite Laminates

Composites behave differently than metals, as mentioned due to their anisotropic nature. Looking at the generalized Hooke’s Law for orthotropic materials we can see that the normal stresses have no relation to the shear strains. Here, an orthotropic material means a material that has at least 2 orthogonal planes of symmetry, where material properties are independent of direction within each plane.

$$\begin{bmatrix} \varepsilon_{xx} \\ \varepsilon_{yy} \\ \varepsilon_{zz} \\ \varepsilon_{yz} \\ \varepsilon_{zx} \\ \varepsilon_{xy} \end{bmatrix} = \begin{bmatrix} \frac{1}{E_x} & -\frac{v_{yx}}{E_y} & -\frac{v_{zx}}{E_z} & 0 & 0 & 0 \\ -\frac{v_{xy}}{E_x} & \frac{1}{E_y} & -\frac{v_{zy}}{E_z} & 0 & 0 & 0 \\ -\frac{v_{xz}}{E_x} & -\frac{v_{yz}}{E_y} & \frac{1}{E_z} & 0 & 0 & 0 \\ 0 & 0 & 0 & \frac{1}{2G_{yz}} & 0 & 0 \\ 0 & 0 & 0 & 0 & \frac{1}{2G_{zx}} & 0 \\ 0 & 0 & 0 & 0 & 0 & \frac{1}{2G_{xy}} \end{bmatrix} \begin{bmatrix} \sigma_{xx} \\ \sigma_{yy} \\ \sigma_{zz} \\ \sigma_{yz} \\ \sigma_{zx} \\ \sigma_{xy} \end{bmatrix}$$

Fig. 1: Stress Strain Relation [5]

$$\boldsymbol{Q}_{ij} = \begin{bmatrix} Q_{11} & Q_{12} & 0 \\ Q_{12} & Q_{22} & 0 \\ 0 & 0 & Q_{66} \end{bmatrix}$$

$$Q_{11} = \frac{E_{11}^2}{(E_{11} - \upsilon_{12} \cdot E_{22})}, \quad Q_{12} = \frac{\upsilon_{12} E_{11} E_{22}}{E_{11} - \upsilon_{12}^2 E_{22}}$$

$$Q_{22} = \frac{E_{11} E_{22}}{E_{11} - \upsilon_{12}^2 E_{22}}, \quad Q_{66} = G_{12}$$

Fig. 2: Q Matrix and Equations [5]

$$\begin{aligned}
\overline{Q_{11}} &= Q_{11}\cos(\theta)^4 + 2(Q_{12} + 2Q_{66})\cos(\theta)^2 \cdot \sin(\theta)^2 + Q_{22}\sin(\theta)^4 \\
\overline{Q_{12}} &= \overline{Q_{21}} = Q_{12}(\cos(\theta)^4 + \sin(\theta)^4) + (Q_{11} + Q_{22} - 4Q_{66})\cos(\theta)^2\sin(\theta)^2 \\
\overline{Q_{16}} &= \overline{Q_{61}} = (Q_{11} - Q_{12} - 2Q_{66})\cos(\theta)^3\sin(\theta) - (Q_{22} - Q_{12} - 2Q_{66})\cos(\theta)\sin(\theta)^3 \\
\overline{Q_{22}} &= Q_{11}\sin(\theta)^4 + 2(Q_{12} + 2Q_{66})\cos(\theta)^2\sin(\theta)^2 + Q_{22}\cos(\theta)^4 \\
\overline{Q_{26}} &= \overline{Q_{62}} = (Q_{11} - Q_{12} - 2Q_{66})\cos(\theta)\sin(\theta)^3 - (Q_{22} - Q_{12} - 2Q_{66})\cos(\theta)^3\sin(\theta) \\
\overline{Q_{66}} &= (Q_{11} + Q_{22} - 2Q_{12} - 2Q_{66})\cos(\theta)^2\sin(\theta)^2 + Q_{66}(\cos(\theta)^4 + \sin(\theta)^4)
\end{aligned}$$

$$\overline{\boldsymbol{Q}_{ij}} = \begin{matrix} \overline{Q_{11}} & \overline{Q_{12}} & \overline{Q_{16}} \\ \overline{Q_{12}} & \overline{Q_{22}} & \overline{Q_{26}} \\ \overline{Q_{16}} & \overline{Q_{26}} & \overline{Q_{66}} \end{matrix}$$

Fig. 3: Transformed Q Matrix and Equations [5]

Looking at each ply from its local coordinate system where its axis are aligned we use the material properties of the laminate, E_1, E_2, G_{12}, v_{12}. These are then used to create the local reduced stiffness matrix Q which is then transformed into the global coordinate system using the laminates angle, theta, to get the transformed reduced stiffness matrix, Q_bar. Finally the A, B, and D matrices can be formed for the full laminate lay-up as they are each calculated by iterating through the laminate stack using the following form.

$$\boldsymbol{A}_{ij} = \sum_{k=1}^{n} \{Q_{ij}\}_n (z_k - z_{k-1})$$
$$\boldsymbol{B}_{ij} = \frac{1}{2} \sum_{k=1}^{n} \{Q_{ij}\}_n (z_k^2 - z_{k-1}^2)$$
$$\boldsymbol{D}_{ij} = \frac{1}{3} \sum_{k=1}^{n} \{Q_{ij}\}_n (z_k^3 - z_{k-1}^3)$$

Fig. 4: A, B, and D matrix equations [5]

$$\begin{bmatrix} N \\ M \end{bmatrix} = \begin{bmatrix} [A] & [B] \\ [B] & [D] \end{bmatrix} \begin{bmatrix} \varepsilon_0 \\ \kappa \end{bmatrix}$$

Fig. 5: Normal Forces and Moments Related to Mid-Plane Strain and Curvature through the A, B, and D matrices [3]

"N is the resultant in-plane force vector, M is the resultant moment vector, epsilon 0 is the mid-plane strain vector, and k is the curvature vector. The A matrix represents the in-plane stiffness of the laminate, the B matrix represents the coupling stiffness, relating the in-plane forces to the out-of-plane bending and twisting deformations, thereby describing the coupling between in-plane and bending responses. The D matrix represents the bending stiffness of the laminate, and relates the bending moments to the curvatures and accounting for the flexural behavior of the laminate" [3]

Expanding the vectors and matrices for the moment in the case of a balanced symmetric layup where the B matrix is zero, the relationship between M and K is as follows,

$$\{Mx\ My\ Mxy\} = [D11\ D12\ D16\ D12\ D22\ D26\ D16\ D26\ D66]\{kx\ ky\ kxy\} \qquad \text{Eq. 1}$$

For a high aspect-ratio wing modeled as a beam, the beam stiffnesses are integral function of the laminate stiffnesses (Aij, Dij). Specifically, the bending-torsion coupling rigidity (K) is directly proportional to the D16 term. It is then clear that by manipulating theta, our ply orientation, we can change our D16 and D26 matrices which allow us to control the twist (k) of the wing under load.

Structural Dynamics

Simplifying the geometry of the wing to a beam allows us to solve the governing equations for composite beams. Unlike isotropic materials where the bending moment depends only on curvature and the torque relies solely on the rate of twisting throughout the beam a composite beam with asymmetric ply orientation has coupled moments and torques that rely on both twisting and curvature. Solving these equations first without considering the aerodynamic effects the wings will experience will allow us to determine two important frequencies that demonstrate exactly how asymmetric orientated plys can help design natural frequencies. In Guo et al. equations one and two are given as,

$$M_b(y,\ t) = EI\frac{\partial^2 h}{\partial y^2} + K\frac{\partial \psi}{\partial y} \quad \text{Eq. 2}$$

$$T(y,\ t) = GJ\frac{\partial \psi}{\partial y} + K\frac{\partial^2 h}{\partial y^2} \quad \text{Eq. 3}$$

Here EI is the bending rigidity and GJ is the torsional rigidity. K is the bending torsional coupling rigidity. For an isotropic material this is zero. Recall also that the shear in a beam is the spatial derivative of the moment. So we can get the equality,

$$\frac{\partial S}{\partial y} = \frac{\partial^2 M_b}{\partial y^2} = \frac{\partial^2}{\partial y^2}\left(EI\frac{\partial^2 h}{\partial y^2} + K\frac{\partial \psi}{\partial y}\right) = EI\frac{\partial^4 h}{\partial y^4} + K\frac{\partial^3 \psi}{\partial y^3}$$

Equation 4

This final form is our elastic restoring force. Similarly the total torque load is the spatial derivative of the internal torque, T(y,t). This gives us,

$$Torque\ Load = \frac{\partial T}{\partial y} = \frac{\partial}{\partial y}\left(GJ\frac{\partial \psi}{\partial y} + K\frac{\partial^2 h}{\partial y^2}\right) = GJ\frac{\partial^2 \psi}{\partial y^2} + K\frac{\partial^3 h}{\partial y^3}$$

Equation 5

This is our elastic restoring torque. Now to ensure we are remaining consistent with the dynamics that would occur in a wing we need to assume that the elastic axis is not coincident with the center of gravity. These two axes will be separated by a distance we call x_a . This allows us to calculate the moments of inertia for both bending and torsion.

$$F_{inertial} = m\frac{\partial^2 h}{\partial t^2} + mx_a\frac{\partial^2 \psi}{\partial t^2}$$

Equation 6

This shows the mass accelerating in h as well as the effect of the offset mass rotating.

$$T_{inertial} = I_a\frac{\partial^2 \psi}{\partial t^2} + mx_a\frac{\partial^2 h}{\partial t^2} \quad \text{Eq. 7}$$

The I_a term is the polar moment if inertia, which is accelerating in torsion, ψ, plus the the offset mass accelerating in bending.

The physical meaning behind these equations and how they relate to composites is shown best by seeing how if K were zero, all interrelated terms drop out, but if K does not equal zero, we can see that when a composite wing undergoes bending it will simultaneously induce a twist. If we take a step back and look again at the assumptions made, we will not that these are the structural dynamics for a beam in a vacuum, or with no aerodynamic effects. So, these equations, for the purpose of understanding the natural frequencies of the beam, are written in their homogenous form.

$$EI\frac{\partial^4 h}{\partial y^4} + K\frac{\partial^3 \psi}{\partial y^3} + m\frac{\partial^2 h}{\partial t^2} + mx_a\frac{\partial^2 \psi}{\partial t^2} = 0$$

$$-GJ\frac{\partial^2 \psi}{\partial y^2} - K\frac{\partial^3 h}{\partial y^3} + I_a\frac{\partial^2 \psi}{\partial t^2} + mx_a\frac{\partial^2 h}{\partial t^2} = 0$$

Equations 8 & 9

We now assume that the wing vibrates at a natural frequency, ω, that relates to a specific mode shape that correlates the frequency to the bending displacement and torsional rotation. Taking $h(y, t)$ as the bending displacement, and $\psi(y, t)$ as the torsional rotation this can be written as,

$$h(y, t) = H(y)e^{i\omega t} \qquad \psi(y, t) = \Psi(y)e^{i\omega t}$$

Equations 10 & 11

If we now differentiate with respect to time twice, we can substitute these equations back into our harmonic equations.

$$EI\frac{\partial^4 H}{\partial y^4} + K\frac{\partial^3 \Psi}{\partial y^3} - \omega^2 mH - \omega^2 mx_a\Psi = 0$$

$$-GJ\frac{\partial^2 \Psi}{\partial y^2} - K\frac{\partial^3 H}{\partial y^3} - \omega^2 I_a\Psi - \omega^2 mx_a H = 0$$

Equations 12 & 13

Assuming the solution to these ODE's takes the form of $H(y) = C_1e^{\lambda y}$, $\Psi(y) = C_2e^{\lambda y}$, we can substitute these equations into matrix form and show that for a non-trivial solution the determinant of the resulting matrix must be equal to 0.

$$\begin{bmatrix} EI\lambda^4 - m\omega^2 & K\lambda^3 - mx_a\omega^2 \\ -K\lambda^3 - mx_a\omega^2 & -GJ\lambda^2 - I_a\omega^2 \end{bmatrix}\begin{bmatrix} C_1 \\ C_2 \end{bmatrix} = \begin{bmatrix} 0 \\ 0 \end{bmatrix}$$

Equation 14

The determinant of this matrix results in a sixth order polynomial, which solving gives six roots, and the general solution for the mode shape is a linear combination of these six roots, of the form, $H(y) = \sum_{i=1}^{6} C_i e^{\lambda_i y}$, where λ, represents the wave number, characterizing how the mode shape varies along the span.

To solve for the natural frequencies, ω, we must apply the boundary conditions of the cantilever wing, where the displacement, slope, and twist at the root is zero and the moment, shear force, and torque at the tip is zero. In Guo, et al. the Wittrick-Williams algorithm is used to solve these natural frequencies. This essentially summarizes the mathematics of how to find the natural frequencies in a composite wing but does not necessarily fully explain why composites are useful here. The system shown yields two sets of natural frequencies. If K = 0, an isotropic material, then the matrix diagonalizes and only pure bending and pure torsion modes are left. For a composite where K is not 0 then the matrix would be completely populated and it can be shown that in the modes there are mostly bending terms but also terms that include induced twist from the composite material. This is what counteracts flutter forces as will be better explained in the next section regarding the flutter mechanisms.

4. Aeroelastic Modeling: The Flutter Mechanism

The exact stability of the wing is defined by the determinant of the dynamic stiffness matrix, as derived by Guo et al.

$$\{K_D(\omega) - \frac{\rho V^2}{2}[QA]_R + i\omega[D] + i\frac{\rho V^2}{2}[QA]_I\}\{q\} = 0$$

Equation 15

This equation, while precise, is extremely complex and computationally intensive especially when trying to optimize wing design. To derive a function for the ply orientation of composites, we simplify this into the Quasi-Steady model used by Dinulovic.

Before implementing the quasi-steady assumption, recall how the bending and torsion occurs during flight and using newtons second law, these will be the reaction forces to the induced aerodynamic forces. This means we can set our bending terms ($\frac{\partial S}{\partial y}$ and $F_{inertial}$) equal to the lift. Similarly, the torsion effects through the wing will be the reaction force to the aerodynamic moment or pitching of the wing. Written out fully these expressions look like,

$$EI\frac{\partial^4 h}{\partial y^4} + K\frac{\partial^3 \psi}{\partial y^3} + m\frac{\partial^2 h}{\partial t^2} + mx_a\frac{\partial^2 \psi}{\partial t^2} =- Lift$$

$$GJ\frac{\partial^2 \psi}{\partial y^2} + K\frac{\partial^3 h}{\partial y^3} + I_a\frac{\partial^2 \psi}{\partial t^2} + mx_a\frac{\partial^2 h}{\partial t^2} = M_{oment}$$

Equations 16 & 17

This will quickly become a more complex system once we introduce the lift term completely as it has interdependence on the geometry of the wing. To overcome this problem, we make the quasi-steady assumption where we assume, "In quasi-steady flutter, the frequency of vibration related to the flapping and twisting of the structure is considerably lower compared to its linear flight speed." [3] Meaning we can negate flutter due to complex geometry changes in the wing.

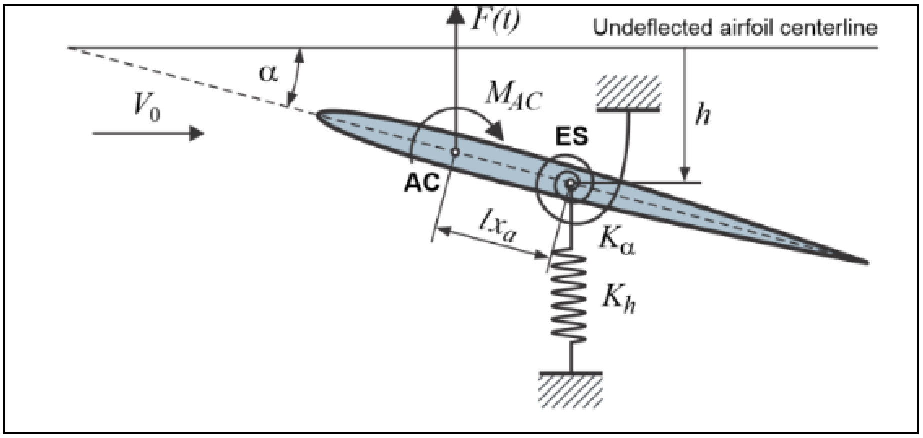

Fig. 6: 2 DOF section view of thin airfoil used for quasi-steady assumption and simplification of aeroelastic effects [3]

While Guo et al. utilize a continuous beam model (PDE) to capture the spanwise stiffness coupling, Dinulović simplifies this into a 2 DOF 'typical section' model (ODE). To bridge these, we use the natural frequencies derived from the rigorous Guo model to define the equivalent spring stiffnesses, K_h, K_α, required for the Dinulović flutter optimization. The spring constant terms here are not arbitrary either, they are actually directly related to the previous analysis in Guo et al. as they are given by the following equations based on the natural frequencies of our wing (simplified as a beam)

$$K_h = m\omega_h^2 \qquad K_a = I_a\omega_a^2$$

Equations 18 & 19

The simplified lift equation from Dinulovic that makes the quasi-steady assumption is formed by,

$$L = \frac{1}{2}\rho V^2 S C_{La}\alpha_{eff} \qquad \alpha_{eff} = \psi + \frac{\dot{h}}{V}$$

Equations 20 & 21

This means we will use a modified version of the equations derived in Dinulovic and the quasi-steady assumption to simplify the problem. Dinulovic assumes that the elastic axis and the center of gravity are coincident, hence why his equations do not have an Sa term (static moment). He did this to isolate the effect of coupling frequencies and show that through aeroelastic forces alone flutter can occur, and that by separating these frequencies we can increase flutter speed. With our assumption that these axes are not coincident, so the equations are,

$$m\ddot{h} + S_\alpha\ddot{\psi} + K_h = - L$$

$$I_\alpha\ddot{\psi} + S_\alpha\ddot{h} + K_\alpha\psi = M_{ac} + L * e$$

Equations 22 & 23

Here we have terms $S_\alpha \ddot{h}$ and $S_\alpha \ddot{\psi}$, which represent the internal coupling, where S_α is the static moment defined as $S_\alpha = mx_{cg}$.

Rearranging these equations into matrix form it shows where the instability is coming from. The aerodynamic forces contribute to the instability as their matrices have off-diagonal terms. Written out,

$$\left[m\, S_a\, S_a\, I_a\right]\left[\ddot{h}\ \ddot{\psi}\right] + \frac{1}{2}\rho V^2 SC_{La}\left[\frac{1}{V}\ 0\ \frac{-e}{V}\ 0\right]\left[\dot{h}\ \dot{\psi}\right] + \left(\left[K_h\ 0\ 0\ K_\alpha\right] + \frac{1}{2}\rho V^2 SC_{La}[0\ 1\ 0\ -e]\right)[h\ \psi] = 0$$

Equation 24

Solving the determinant of this system for the critical condition (where total damping becomes zero) yields a closed-form expression for the flutter speed, as derived by Dinulović,

$$V_f = \frac{A^*}{2}\sqrt{\omega_\psi^2 - \omega_h^2} \quad \text{Eq. 25}$$

In this equation A* is defined as being non-structural parameters such as chord length, density, etc. The important part is that it describes the relationship between the two natural frequencies our wing is based on, the torsional natural frequency ω_ψ^2, and the bending natural frequency, ω_h^2. It also shows that our goal should be to separate these natural frequencies as much as possible in order to give the greatest V_f. In Dinulović this is stated as maximizing delta $\Delta = \omega_\psi^2 - \omega_h^2$. This can be done by manipulating the ply orientation, theta, to change the stiffness coupling of the wing, and therefore vary the eigenvalues increasing delta, and therefore increasing the flutter speed.

5. Design Constraints

In the last section we discussed the physics behind aeroelastic tailoring of composite aircraft wings, but the engineering point of view is equally necessary to understand the realities of this design method. In order to maximize the bending-torsion coupling, K, asymmetric ply layups are necessary but have important manufacturing and structural considerations.

Asymmetric layups are much more difficult to manufacture because the same properties that allow them to couple bending and torsion, as well as extension-bending coupling, make the cure cycle a difficult process as this means they are more likely to warp due to thermal properties also being coupled. Additionally, as seen in the figure below, a results table form Guo et al., shows that the optimization he used for flutter originally resulted in a stress ratio of 2.38. This means there was a 238% increase in the maximum stress in the composite fibers, and would likely cause the wing to fail structurally. In his second stage, Guo constrained the optimization by tapering the wing box width along the span of the wing. This maintained the flutter optimization in stage 1 but ensured that the wing would be structurally sounds as well.

Optimal stage	Wing box width of each of the following sections (from root)										Stress ratio R_s	Weight ratio R_W	Flutter ratio R_V
	1	2	3	4	5	6	7	8	9	10			
Stage 1	0.80	0.80	0.80	0.80	0.80	0.80	0.80	0.80	0.80	0.80	2.38	1.00	1.00
Stage 2	0.97	0.92	0.87	0.82	0.82	0.73	0.68	0.64	0.59	0.54	1.00	0.87	1.00

Fig. 7: Guo et al. results table from stage 1 and 2 optimization strategies

6. Modern Optimization Techniques

Guo's methods for solving are entirely calculus based, which, although helps to ground the engineering in physics and the governing equation, is not computationally efficient and also has the possibility of getting stuck on local maxima. In contrast, a more modern approach to solving problems like aeroelastic tailoring of composite laminates, are like that of Dinulović and the fast tree regression algorithm he used.

"The Fast Tree Algorithm is a powerful optimization tool that utilizes tree-based data structures to efficiently search through the vast solution space of fiber orientations." [3] This method consisted of starting with a seed data set of 58 different laminates and then using FEM to get the Δ value described earlier. A machine learning algorithm was then trained on these results and used to scan many other possible laminate stacks to identify the best one. This method works better for aeroelastic tailoring because composites layups are often discrete angles, making gradient based methods, like Guo's, struggle.

"It is postulated that flutter, indicative of plate instability, occurs when the structure's damping value diminishes to zero. Hence, … it is evident that the damping for the non-optimal lay-up reaches zero at speeds of 23 m/s. In contrast, for the optimal configuration obtained through the methodology described in this research, the flutter velocity is 30 m/s, marking a notable increase of over 23%." This shows very promising results and

7. Real Engineering Applications

The theoretical coupling mechanism, K, was validated by the Grumman X-29 technology demonstrator. The X-29 utilized a forward-swept wing, a configuration historically plagued by aeroelastic divergence. By tailoring the composite wing skins with specific asymmetric ply orientations, engineers created a passive restoring moment. Lift induced bending created a nose-down twist that counteracted the aerodynamic instability. This application successfully demonstrated that the bend-twist coupling term D16 is sufficiently powerful to stabilize an otherwise unstable wing.

Fig. 8: the Grumman X-29 Demonstrator in flight

Moving beyond fixed material properties, the Variable Stiffness Spar (VSS) concept investigated by Florance et al. at NASA Langley demonstrates the feasibility of active structural tailoring. This experiment simplifies the system, but proves the use of a variable D16 matrix term by mechanically rotating spar to actively vary the structural properties of the wing with a change in spar angle, theta. The VSS employs a mechanical rectangular steel spar capable of rotating 90 degrees within the wing structure [7]. In the "vertical" orientation, the spar maximizes the area moment of inertia, I, providing high bending stiffness; in the "horizontal" orientation, the spar reduces stiffness, effectively softening the wing to alter its aeroelastic response.

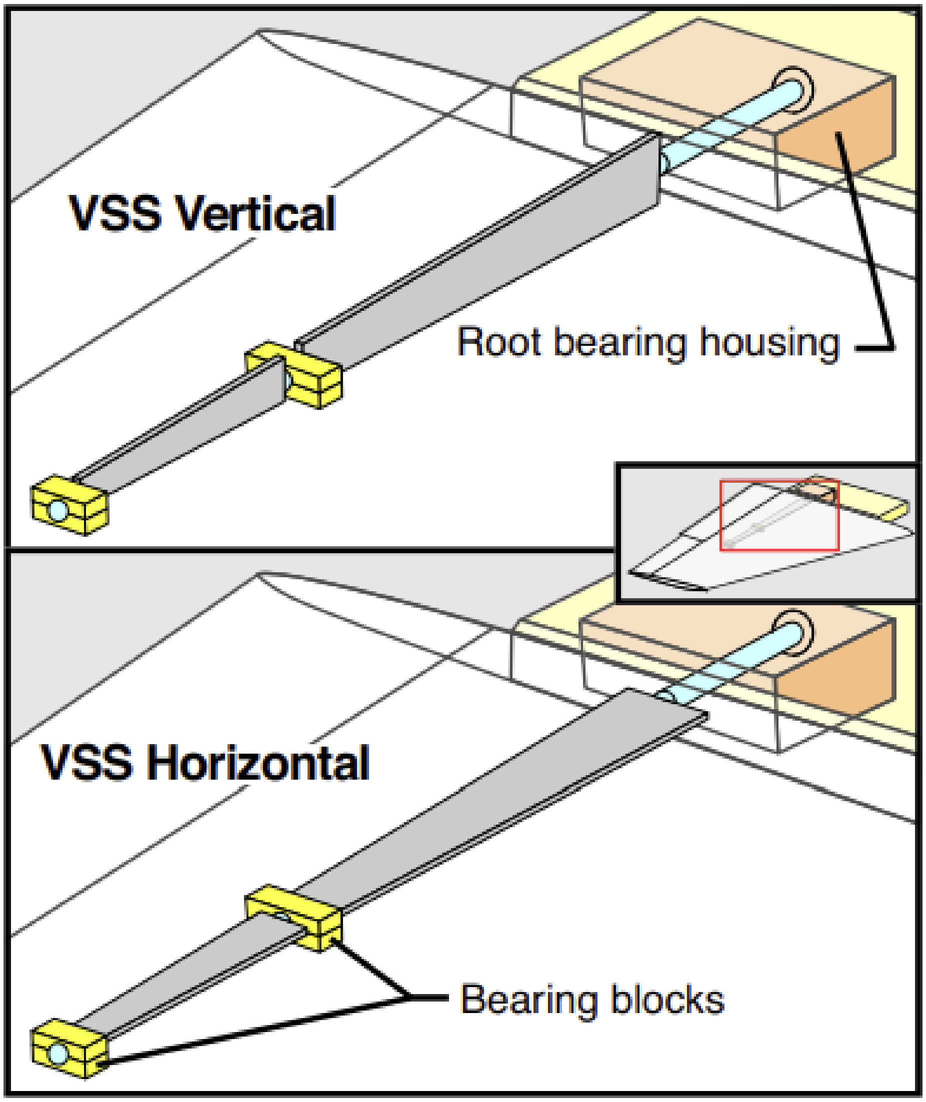

Fig 9: Diagram of the VSS Spar and Wing [7]

Wind tunnel tests in the Transonic Dynamics Tunnel (TDT) confirmed that rotating the spar altered the wing's modal frequencies and static aeroelastic characteristics, specifically affecting the lift curve slope, $C_{L\alpha}$, in the transonic regime and the rolling moment effectiveness ($C_{L\delta}$) of the leading-edge outboard flaps [7]. While the specific wind tunnel model was constrained by safety factors that resulted in higher-than-desired stiffness, the experiment successfully validated that mechanical alteration of the wing's internal structure can actively manipulate aerodynamic derivatives in flight.

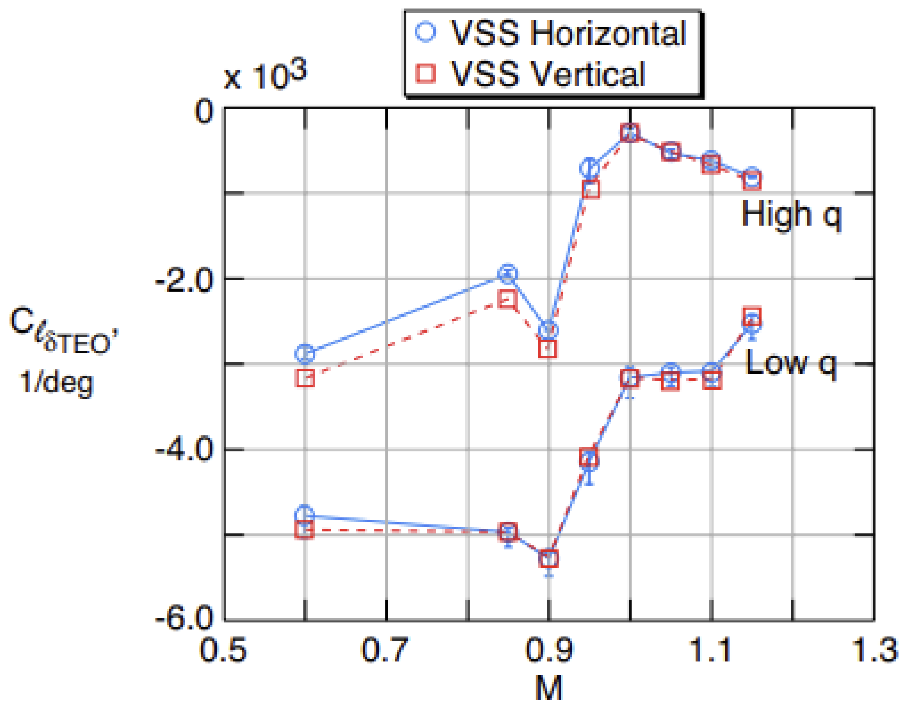

Fig 10: Control Surface Effectiveness for Varying Mach Numbers on the VSS Wing [7]

Additionally, the study by Popelka et al. on the V-22 Osprey presents a definitive case for the necessity of composite aeroelastic tailoring in high-speed, flexible aircraft design. The core engineering challenge was the need to reduce the wing thickness-to-chord ratio from a stability-driven 23% to a more aerodynamically efficient 18%, a modification that naturally lowers the structural stiffness and precipitates proprotor whirl flutter instability [6].

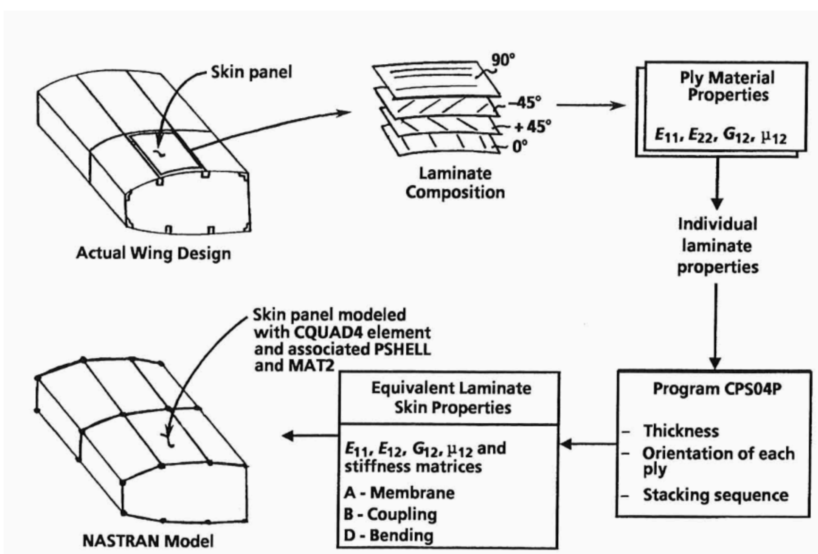

Fig 10: Composite Laminate Optimization Method for V-22 Osprey [6]

The fundamental strategy employed was the passive manipulation of the wing box's stiffness matrix using unbalanced composite laminates, as seen in figure 11. By biasing the wing skin layups (using a 70% +/- 45-degree blend), the designers introduced a calculated material anisotropy that generates specific out-of-plane coupling terms, notably the extension-shear coupling represented by the A16 and A26 terms. This coupling ensures that when the wing undergoes vertical bending, the primary driver of the flutter mode, the resulting in-plane stress fields induce a nose-down torsional twist. This passive structural mechanism counteracts the destabilizing aerodynamic moment, successfully raising the flutter speed margin of the thinner wing.

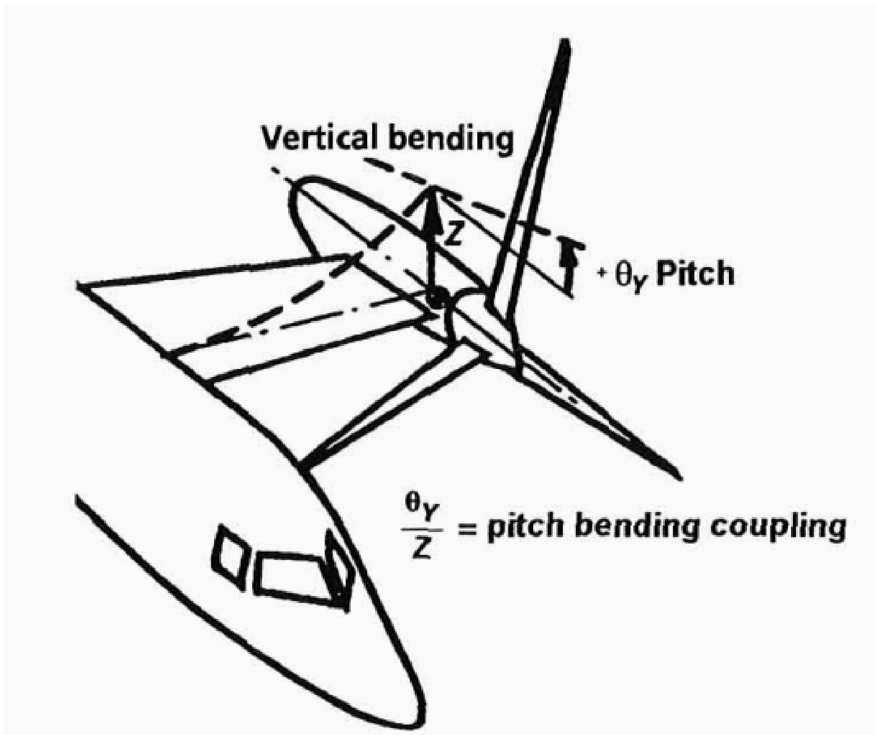

Fig 11: Pitch-Bend Coupling Diagram for Tiltrotor System [6]

While composite tailoring effectively addresses the stability of the symmetric wing beam wise bending (SWB) mode, the V-22 analysis highlights a complex and often-overlooked trade-off involving conflicting design requirements. The same highly unbalanced laminates that introduce the pitch-bending coupling cause a significant reduction in the effective torsional stiffness, GJ, of the wing box. This degradation of torsional resistance subsequently destabilizes the symmetric wing chordwise bending (SWC) mode, leading to an unacceptable reduction in its divergence speed or its low-frequency flutter boundary. The final design solution could not rely solely on skin tailoring. Instead, a hybrid approach was required: the tailored skins were maintained for SWB stability, but the structural layout was optimized by transferring material from internal stringers to the spar caps. This optimized cross-sectional area distribution restored the necessary chordwise bending stiffness, EI of the chord, to meet the SWC stability requirements without nullifying the gains achieved in the beam wise mode, ultimately resulting in an 18% wing that demonstrated greater overall stability than the original, thicker V-22 wing.

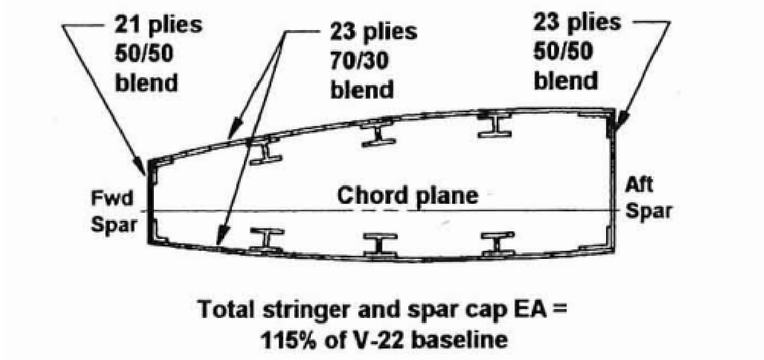

Fig. 17. Final 18% *t/c* three-stringer tailored wing configuration.

Fig 12: Final Composite Skin Layout for V-22 Osprey Wing [6]

8. Conclusion

The integration of composite materials into aircraft wing design represents a shift from purely structural sizing to active aeroelastic tailoring. By exploiting the anisotropic nature of fiber-reinforced laminates, specifically the bending-torsion coupling, K, engineers can design wings that passively alleviate aerodynamic loads.

This research looked at two distinct mathematical frameworks to validate this approach. Utilizing the continuous beam model derived by Guo et al. to calculate the natural frequencies of a composite wing, accounting for the unique stiffness coupling terms D_{16}. Then bridging this structural model with the quasi-steady aeroelastic model used by Dinulović, proving that the flutter speed is proportional to the separation of the torsional and bending natural frequencies, $\Delta = \omega_{\psi}^2 - \omega_h^2$.

While optimization strategies like the Fast Tree Regression algorithm have demonstrated potential flutter speed increases of over 23%, this study highlights that such gains must be balanced against structural realities. Asymmetric laminates, while theoretically optimal for flutter, introduce manufacturing challenges and static strength penalties (stress ratios > 2.0). Therefore, the future of wing design lies in constrained aeroelastic tailoring: utilizing symmetric, unbalanced laminates to maximize frequency separation while maintaining the structural integrity required for safe flight.

Sources

1. Njuguna, J. (2007). Flutter prediction, suppression and control in aircraft composite wings as a design prerequisite: A survey. *Structural Control and Health Monitoring*, *14*(5), 715–758. https://doi.org/10.1002/stc.170

2. Guo, S. J., Bannerjee, J. R., & Cheung, C. W. (2003). The effect of laminate lay-up on the flutter speed of composite wings. *Proceedings of the Institution of Mechanical Engineers. Part G, Journal of Aerospace Engineering*, *217*(3), 115–122. https://doi.org/10.1243/095441003322297225

3. Dinulović, M., Bengin, A., Krstić, B., Dodić, M., & Vorkapić, M. (2024). Flutter Optimization of Carbon/Epoxy Plates Based on a Fast Tree Algorithm. *Aerospace*, *11*(8), 636. https://doi.org/10.3390/aerospace11080636

4. Pavan Kishore, M. L., Madhavi, B., Pati, P. R., Pugazhenthi, R., Giri, J., Sathish, T., & Parthiban, A. (2024). Free vibration analysis of composite aircraft wing. *Interactions*, *245*(1), 1–11. https://doi.org/10.1007/s10751-024-01976-0

5. A summary of classical lamination theory defining the laminate. (n.d.). https://wstein.org/edu/2010/480b/projects/05-lamination_theory/A summary of Classical Lamination Theory.pdf

6. Popelka, D., Lindsay, D., Parham, T., Berry, V., & Baker, D. J. (1997). Results of an Aeroelastic Tailoring Study for a Composite Tiltrotor Wing. *Journal of the American Helicopter Society*, *42*(2), 126–136. https://doi.org/10.4050/JAHS.42.126

7. Florance, J. R., Heeg, J., Spain, C. V., Ivanco, T. G., Wieseman, C. D., & Lively, P. S. (2004). *Variable Stiffness Spar Wind-Tunnel Model Development and Testing*. https://ntrs.nasa.gov/citations/20040066092